

High Pore Density Polyimide Membrane Production by PS Laser Pulses

Pierre Lorenz*, Martin Ehrhardt, and Klaus Zimmer

Leibniz Institute of Surface Engineering (IOM), Permoserstr. 15, D-04318 Leipzig, Germany

**Corresponding author's e-mail: pierre.lorenz@iom-leipzig.de*

High pore density membranes exhibit various applications, especially in microfiltration, bioseparation, microbiology and medicine. The laser ablation process allows the fabrication of membranes with high pore density and pore diameter in the μm and sub- μm range. Ultrashort laser pulses allows the efficient and precise fabrication of pores in polymer foils due to the high repetition rate and the low thermal effects. Polyimide (PI) foils with a thickness of $13\ \mu\text{m}$ were irradiated by ultraviolet picosecond laser radiation. The fabricated membranes have a pore diameter from $\sim 0.7\ \mu\text{m}$ to $75\ \mu\text{m}$ in dependence on the laser parameter. Furthermore, high pore density up to $\sim 23500\ \text{mm}^{-2}$, high-precision pores with standard deviation of pore diameter less than 10 % and high areal pore density up to $\sim 12\ %$ were achieved. The detailed analysis of the pore size at the front and rear side in correlation to the laser parameter enable an empiric description of the pore size – laser parameter dependency which allows the optimisation of the pore density.

DOI: 10.2961/jlmn.2022.01.2002

Keywords: ps-laser, drilling, membranes, polyimide, PI

1. Introduction

Porous polymeric membranes are needed in different fields of application such as in microfiltration, bioseparation, microbiological screening and biomedical separation application. Various techniques enable the fabrication of polymeric membranes by determined and random processes technologies [1]. Narrow distributions of the pore size and high pore densities always requested for innovative applications. Hence, a direct writing process is studied to realize micron sized thin foil membranes.

Short and ultra-short pulse laser irradiation of polymers can cause laser ablation resulting from the decomposition of the material due to disintegration of hydrocarbon chains. Laser ablation is a well-established tool for surface patterning, structuring and modification of polymer films and foils [2-9]. The ablation process was already studied for different polymers like polytetrafluoroethylene (PTFE), polyether ether ketone (PEEK), polyethylene terephthalate (PET) and polycarbonate (PC) [2, 10]. Polyimide (PI) is a well-qualified polymer for various applications due to its exceptional optical, chemical, thermal and electrical properties [10]. The laser ablation process of PI was studied for very different laser sources with pulse durations from femtosecond (fs) to nanosecond (ns) and with wavelengths ranging from infrared to ultraviolet [4, 7, 8, 11-16]. The ablation of polymers can be of photothermal or photochemical nature [5]; both cause finally the decomposition of the polymer and the formation of gaseous products. The very fast laser ablation process is accompanied by secondary processes such as heating of the substrate material near the ablation pit, the formation of an ablation plume with high pressures and shock waves, as well as the redeposition of ablated material [3, 5]. Blind, deep holes and through-holes (micro-drilling) can be fabricated by laser ablation in polymer foils using ns- [17, 18],

ps- [19] and fs-laser radiation [12]. The fabrication of periodic through-holes patterns and therefore the production of porous membranes from functional polymer [11] can be achieved by repetitive micro-drilling. A parallel fabrication of dense holes arrays by laser ablation can be realized by mask projection or laser interference patterning. However, specialized optical set-ups are needed to achieve the required high resolution on sufficient large fields. This study focuses on the fabrication of porous polyimide membranes with adaptable holes properties like hole size and hole density using ultraviolet ps-laser ablation. A hole size in the sub- μm and μm range was used which is especially very interesting for cell separation application [20, 21]. The focus of the study is the high-precision drilling of hexagonal hole arrays with a high areal pore density, and a low deviation of the pore diameter in PI foils using gaussian UV ps laser radiation. Further, the front and rear side diameter was systematically analyzed dependent on the laser parameter and the hole distance.

2. Experimental Setup

The laser drilling of polyimide (PI) foils was studied with the aim of the fabrication of holes arrays and porous membranes, respectively. Commercial $13\ \mu\text{m}$ polyimide foils (DuPont Kapton HN) were used because the thickness represents a good compromise between mechanical stability and the goal of achieving high hole densities. Therefore, the PI foils were fixed on the workstation's stage with a vacuum chuck based on porous ceramic. The polyimide was irradiated by the third harmonic of a Nd:YVO₄ laser with a wavelength of 355 nm and a pulse duration of 12 ps. The laser radiation is linearly polarized. The repetition rate was fixed to 100 kHz.

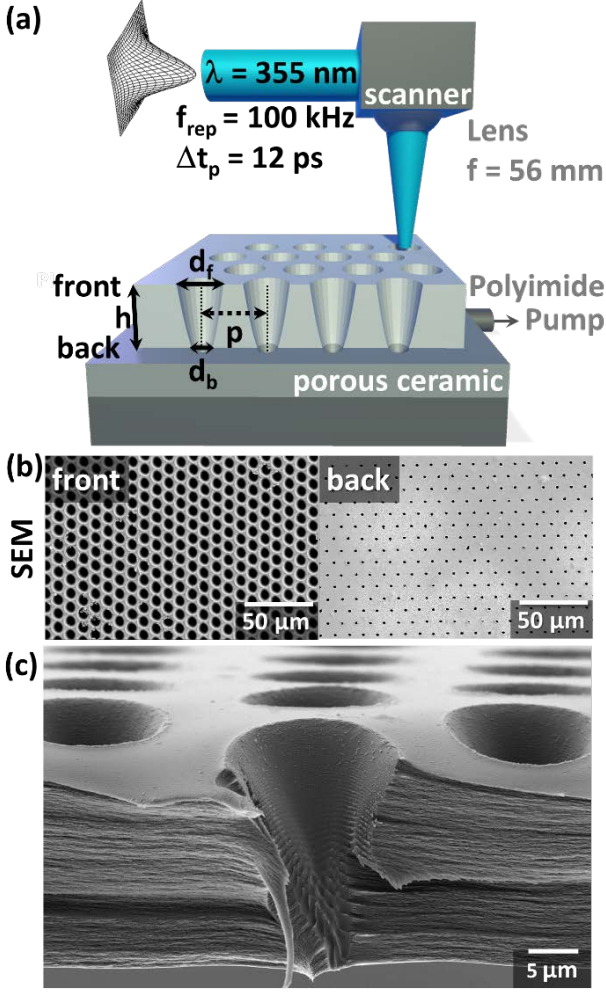


Fig. 1 (a) Schematic illustration of the experimental set-up
 (b) Top view SEM images of front and rear side of a ps-Laser structured PI
 (c) Exemplary SEM image of cross section of a laser irradiated PI foil (Note: For a better visualization of the hole shape an image of a 25 μm PI foil is shown here.).

The laser that is embedded in a workstation (micro-STRUCT from 3D Micromac) is focused on the sample surface by a f-theta lens with a focal length of 56 mm. The laser spot was moved across the sample surface using a galvo scanner (see Fig. 1). The Gaussian radius of the laser spot ω_g was determined by Liu's method [22] to be $(5.7 \pm 0.8) \mu\text{m}$. The laser-treated surfaces were analyzed by optical (OM) and scanning electron microscopy (SEM). For SEM imaging, the samples were covered by magnetron sputtering with a ~ 10 nm gold layer to excluded charging effects. In the first series of experiments, the PI foil was irradiated with various laser energies E and number of laser pulses N where the distance of the irradiated spots p is much larger than the laser spot size to excluded interaction effects between subsequent laser irradiations. At suitable laser parameter, the laser irradiation results in a complete penetration of the PI foil and the formation of a pore with a circular front side hole and rear side hole geometry from circular-like to geometries with significant deviation from the circular geometry dependent

on the laser parameter. The laser-drilled pores are mainly defined by a larger hole diameter on the front side (d_f , irradiated side) and a smaller hole diameter on the rear side (d_b) of the foil (see Fig. 1). The laser-ablated pores are tapered having approximately a conical shape (see Fig. 1 (c)) with a smooth side wall near the front side that become rough near the exit hole. The pores density ρ_h depends on the pore distance p and can be estimated for hexagonal pore distributions from geometric considerations (see Fig. 2) to be:

$$\rho_h [m^{-2}] = \frac{N_h}{A} = \frac{2}{\sqrt{3} \cdot p^2} \approx \frac{1.15}{p^2} \quad (1)$$

The areal pore density $\rho_{h,A}$ is dependent on the pore distance p as well as on the rear side hole diameter d_b . The exit hole diameter is relevant for the calculation of the areal pore density of laser drilled, porous foil membranes due to the conicity of the holes. The areal pore density can be estimated, with N_h : number of holes per unit cell, A : area of unit cell, according to:

$$\rho_{h,A} [\%] = 100 \% \cdot \frac{N_h \cdot \frac{\pi}{4} d_b^2}{A} \approx 90.7 \% \cdot \left(\frac{d_b}{p}\right)^2 \quad (2)$$

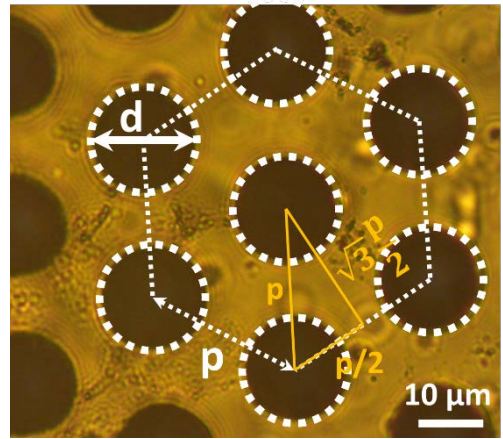


Fig. 2 Exemplary optical image of ps-laser irradiated PI surface including the sketch of the hexagonal pattern.

3. Experimental results and Discussion

3.1 Single holes

The PI foils were irradiated with different numbers of laser pulses and varying laser pulse energy in order to study the laser ablation process. The ablation rate, the ablation threshold, the front and rear side hole diameter was analyzed based on the optical images and are depicted in Fig. 3 for instance.

- **Ablation rate**

The required number of laser pulses N_{req} for foil penetration decreases with increasing of laser pulse energy. The averaged ablation rate Δz defined by $\Delta z = h/N_{req}$ was determined from the required number of laser pulses N_{req} for penetration of the foil with the thickness h . The so determined ablation rates in dependence on the laser pulse energy are shown in Fig. 3 (b). The ablation rate increase with increasing laser pulse energy. At low laser pulse energy from $0.08 \mu\text{J}$ to $\sim 6 \mu\text{J}$, the ablation rate increases logarithmic with

increasing laser pulse energy E and can be fitted with (see black line in Fig. 3b):

$$\Delta z(E) [\mu\text{m}] \approx 0.217 \cdot (\ln(E[\mu\text{J}]) + 4.13) \quad (3)$$

For laser pulse energies above $\sim 6 \mu\text{J}$, the ablation rate increases almost linearly with increasing laser pulse energy (see Fig. 3 b – blue line). The experimental data can be approximated by:

$$\Delta z(E) [\mu\text{m}] \approx 0.186 \cdot E[\mu\text{J}] + 0.00544 \quad (4)$$

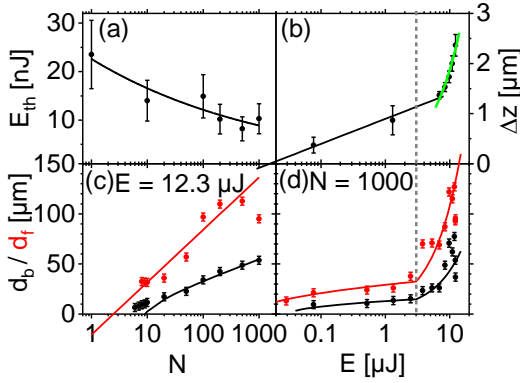


Fig. 3 (a) Laser ablation threshold E_{th} dependency on the number of laser pulses N based on the Liu plot of the front side hole diameter (black line: fit based on Eq. 5)

(b) Ablation rate Δz of polyimide dependent on the laser pulse energy E (black square: experimental results, green line: linear trend (Eq. 4), black line logarithmic trend (Eq. 3))

(c) Front side hole diameter d_f and rear side hole diameter d_b on the polyimide foil at a laser pulse energy $E = 12.3 \mu\text{J}$ dependent on the number of laser pulses N (black and red line fit based on Eq. 6-8)

(d) Front side hole diameter d_f and rear side hole diameter d_b of the polyimide foil at a number of laser pulses of $N = 1000$ dependent on the laser pulse energy E (black and red line fit based on Eq. 6-8)

In agreement with former experimental results for UV ns laser ablation two different ablation mechanism of PI were identified. The ablation process is governed at low laser fluence by photochemical processes and at high laser fluences by a photothermal mechanism [23]. At one hand the influence of non-linear effects increases with higher laser pulse energy especially for ultrashort laser pulses but at the other hand the higher pulse energy cause increasingly thermal processes; both have strong impact to the observable ablation behavior. The logarithmic ablation rate at low laser pulse energy is related to Lambert–Beer’s law. According to Fig. 3, a penetration depth of $\sim 217 \text{ nm}$ and an effective absorption coefficient of $\delta = 4.6 \mu\text{m}^{-1}$ can be estimated (see Eq. 3). This estimated effective absorption coefficient is in the same order of magnitude than the linear absorption coefficient of PI at room temperature with $\alpha = 2 \mu\text{m}^{-1}$ [24].

• Ablation threshold

Furthermore, the ablation rate measurements (Fig. 3 b) allows the estimation of an ablation threshold $E_{th}^* = 0.016 \mu\text{J}$ (see Eq. 3). The ablation threshold E_{th}^* based on Eq. 3 is defined for multi pulse irradiation. The laser ablation threshold energies E_{th} at defined number of laser pulses were determined by using Liu’s approach [22]. The ablation threshold dependence on the number of laser pulses is shown in Fig. 3 (a). The reduction of the ablation threshold with increasing laser pulse number is called incubation effect and is related to the accumulation of laser-induced material defects or induced by thermal accumulation effects [25]. The influence of the incubation process on the ablation threshold can be empiric described by [26]:

$$E_{th}(N)[\mu\text{J}] \approx E_1 \cdot N^{-\xi} \quad (5)$$

The experimental result (see Fig. 3 (a) black squares) can be described by Eq. 5 with single pulse laser ablation threshold of $E_1 = 22.6 \text{ nJ}$ and incubation coefficient of $\xi = 0.135$.

The multi-pulse ablation threshold E_{th}^* based on Eq. 3 is in good agreement with the ablation threshold based on the Liu plot (see Eq. 5) where an ablation threshold from $\sim 0.023 \mu\text{J}$ (at $N = 1$) to $\sim 0.009 \mu\text{J}$ (at $N = 1000$) was found. The experimental found laser ablation threshold for a single pulse ($N = 1$) implies a laser fluence threshold of $\Phi_{th} \sim 22 \text{ mJ/cm}^2$ for a Gaussian radius of $5.7 \mu\text{m}$. This value is larger than the experimental value of $\sim 6 \text{ mJ/cm}^2$ for ns laser ($\lambda = 355 \text{ nm}$, 2-3 ns) [10] and slightly smaller compared to $30 - 70 \text{ mJ/cm}^2$ for KrF Excimer laser ablation ($\lambda = 248 \text{ nm}$, $\Delta t_p = 25 \text{ ns}$) [4]. Similar to other studies the reduction of the ablation threshold with increasing number was found (see Fig. 3 b) [25, 27-29].

• Front and rear side hole diameter

The hole diameter d_{fb} on the front (f) and rear side (b) increases with increasing number of laser pulses (see Fig. 3 (c)) as well as with growing laser energy (see Fig. 3 (d)). At low laser energy ($E < 3 \mu\text{J}$), the hole diameter increased logarithmic with increasing laser energy. At high laser energy ($E > 3 \mu\text{J}$), the hole diameter increased linear at increasing laser energy.

At low laser energy, the logarithmic behavior of the front side hole diameter is related to the Gaussian energy distribution in the laser spot. With an ideal Gaussian laser beam profile (effective Gaussian radius ω_{eff}) and the pulse number dependent ablation threshold (see Eq. 5), the front side diameter $d_{f,L}$ can be estimated by:

$$d_{f,L}(N, E) \approx \sqrt{2} \cdot \omega_{eff} \cdot \sqrt{\ln(E) - \ln(E_1) + \xi \cdot \ln(N)} \quad (6)$$

With Eq. 6 the experimental found hole sizes can be fitted well for $E < 3 \mu\text{J}$ (see Fig. 3 (c) and (d)). The fit parameters are summarized in table 1. The rear side diameter increases also logarithmically with increasing laser energy, but incubation is different. The experimental results (see Fig. 3 (c) and (d)) can be fitted with Eq. 6 after modification. The rear side diameter for $E < 3 \mu\text{J}$ can be empirically described by:

$$d_{b,L}(N, E) \approx \sqrt{2} \cdot \omega_{eff} \cdot \sqrt{\ln(E) - \ln(E_{th}(N))} \quad (7)$$

with

$$E_{th}(N) \approx e^{\frac{h}{N \cdot m} \cdot n} \quad (7b)$$

and m , n : fit parameter (see Table 1). At high energy ($E > 3 \mu\text{J}$), the experimental behavior can no longer be described by the simple physical motivated approaches, so that an empirically determine function:

$$d_{f/b,H}(E, N) [\mu\text{m}] \approx d_{f/b,L}(E_0, N) + a_{f/b} \cdot (E - E_0) \cdot \ln(b_{f/b} \cdot N) \quad (8)$$

with the fit parameter $a_{f/b}$ and $b_{f/b}$ was used. All fitted data shown as solid lines in Fig. 3 with the fit parameters given in table 1.

Table 1 Summary of the fit parameter Eq. 6-8 see Fig. 3 (c), (d)

$d(N, E)$	$d_f [\mu\text{m}]$	$d_b [\mu\text{m}]$
a [$\mu\text{m}/\mu\text{J}$]	1	2.4083
b	0.05808	0.08829
$E_0 [\mu\text{J}]$	3	3
$\omega_{\text{eff}} [\mu\text{m}]$	9.49	4.9
$E_1 [\mu\text{J}]$	0.0226	
ξ	0.135	
m		0.27
n		3.5

The physical description of the front and rear side diameter (see Eq. 6, 7) allows a qualitative good prediction of the logarithmic behavior at low laser pulse energy ($E < 3 \mu\text{J}$). However, the resulting fit parameters (see table 1), which allows the quantitative description of $d_f(E)$, do not correlated to “real” physical parameter and the empiric equation does not provide by a physical description. At $E > 3 \mu\text{J}$, the front side as well as the rear side hole diameter exhibit a more complex behavior and cannot be described by the easy physical approach. However, the empiric equations Eq. 7 and Eq. 8 allows a good fitting of the d_f and d_b dependencies.

Based on the empirical equations (Eq. 6-8), the geometry of laser-drilled holes can be predicted from the processing parameters. Also the laser processing parameters for specific pores or pores arrays geometries can be estimated enabling a adaption of process parameters to e.g. a different polyimide foil thickness. However, the simple empiric description of the experimental results has limitation in the validity that can be extended by simulations with a suitable physical model using finite element method (FEM) as reported by Lasagni et al. [10] and P. E. Dyer et al. [7].

3.2 Hole arrays / membranes

Based on the results of the single hole drilling experiments, hexagonal-ordered pore arrays were machined. Considering the determined correlations laser process parameters can

predefined that allows the fabrication of membranes with adjustable parameters like pore diameter (rear side hole diameter), pore density, hole shape.

In Fig. 4 (left), exemplary SEM images of hexagonal-ordered holes on the rear side of the PI foil are shown.

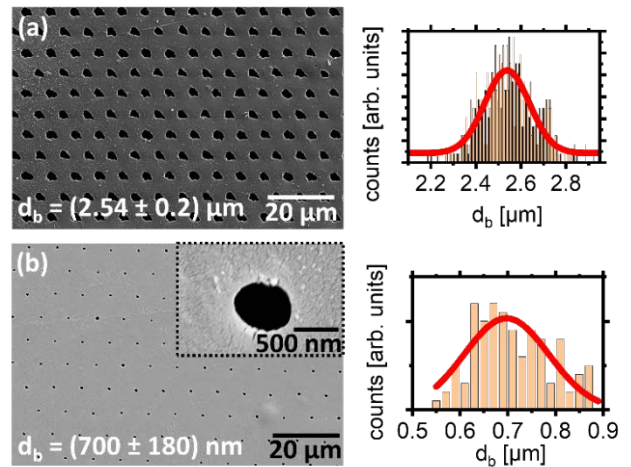


Fig. 4 SEM images (left) and holes diameter histograms (right) of ps-laser drilled 13 μm PI foils.

(a): $N = 150$, $E \sim 0.06 \mu\text{J}$, $p = 7 \mu\text{m}$,

(b): $N = 140$, $E \sim 0.04 \mu\text{J}$, $p = 8 \mu\text{m}$

The related histograms of the holes diameter for two selected arrays are shown in Fig. 4 (right). The array with an average hole diameter of $\sim 2.54 \mu\text{m}$ is achieved at a laser pulse energy of $\sim 0.06 \mu\text{J}$, a number of laser pulses of 150 and a hole distance of $7 \mu\text{m}$ (see Fig. 4 (a)). The presented array features a pores density of 23469 mm^{-2} and an areal pore density of 11.9% . The hole diameter histogram shows a Gaussian distribution with a standard derivation of $\Delta d_b = 0.2 \mu\text{m}$. In general, a typical standard derivation of $\Delta d_b \lesssim 10 \%$ is found for rear side hole diameter $d_b > 1 \mu\text{m}$. The reduction of the laser pulse energy and the number of laser pulses allows the fabrication of pore arrays with smaller rear side diameters down to the sub- μm range.

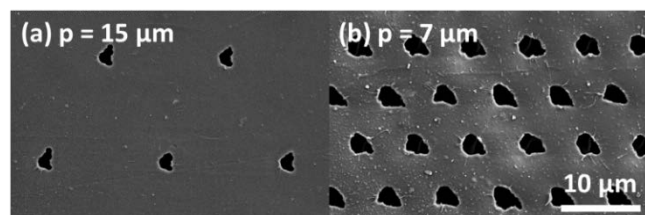


Fig. 5 SEM images of the rear side of a ps-laser irradiated 13 μm PI foil ($N = 150$, $E \sim 0.06 \mu\text{J}$) at a pore distance of $p = 15 \mu\text{m}$ (a) and $p = 7 \mu\text{m}$ (b), respectively.

In particular, the array seen in Fig. 4 (b) machined at a laser pulse energy of $\sim 0.04 \mu\text{J}$ and $N = 140$ features an average rear side hole diameter of $700 \pm 180 \text{ nm}$, a pores density of 17969 mm^{-2} , and an areal pore density of 0.7% . Furthermore, the influence of the pore diameter (rear side hole diameter) from the pore distance was studied. For hole dis-

tances smaller than the front side hole diameter, the pore distance result in the reduction of the average thickness of the foil and in consequence in an increase of the rear side hole diameter (see Fig. 5(a, b)). A further decreasing of the pore distance results in a complete destruction of the PI foil at the same laser processing parameters applied.

• **Pore diameter**

Based on the single hole experiments, it could be shown that the pore diameter / rear side hole diameter can be varied over two order of magnitudes from $\sim 0.7 \mu\text{m}$ to $\sim 75 \mu\text{m}$ due to the variation of the laser parameter (see Fig. 3 (c) and (d)). At a pore distance $p > d_f$, the d_f and d_b of the resultant membrane can be described by Eq. 6-8 with the fit parameter summarized in Table 1. At $p < d_f$, the predicted d_b is smaller than the experimental found d_b due to the overlap of the holes on the front side (see Fig. 7). The overlap result to an overall thinning of the foil (see Fig. 7). At suitable laser parameter, the laser ablation process allows the fabrication of pore arrays with high-precision rear side hole diameters. The accuracy of the hole diameter is most likely defined by local inhomogeneity of the polyimide like foil thickness and of the chemical composition as well as mechanical effects limited the accuracy of the hole diameter (see section “hole shape”). The production of smaller rear side hole diameter can be most likely produced by using microscopic optics which allows the usage of laser beams with smaller Gaussian radius. However the size, precision and quality of the holes is also limited from secondary effects of laser ablation such as mechanical effects (see section “hole shape”) causing material rupture or thermal effects related to heat accumulation and thermal diffusion.

• **Pore density**

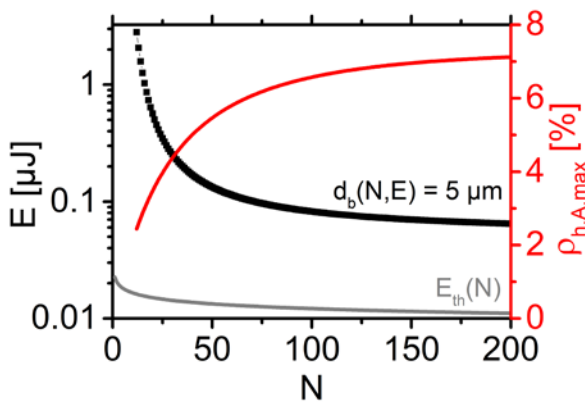


Fig. 6 (black curve) Estimated necessary laser energy E dependent on the number of laser pulses N for the fabrication of a pore with a rear side diameter of $5 \mu\text{m}$ based on Eq. 6-8 taking into account the fit parameter summarized in table 1. (red curve) Estimated maximum achievable areal pore density $\rho_{h,A,max}$ dependent on the necessary number of laser pulses based on Eq. 2 with $p = d_f$ (calculated by Eq. 6-8) (grey curve) Estimated ablation threshold based on Eq. 5 dependent on the number of laser pulses

The areal pore density $\rho_{h,A}$ is given by Eq. 2, depends on the rear side hole diameter d_b and the pore distance p , and increases with small p/d_p ratios. However, the experimental results of single hole drilling show that the rear and front side hole diameter is linked which limits the achievable areal pore density due to the gradual thin down the foil thickness. The maximum areal pore density $\rho_{h,A,max}$ can be estimated assuming the minimum pore distance that is given by the front side hole diameter and the validity of Eq. 6-8 over the entire considered parameter field. The calculated maximum areal pore density at $d_b = 5 \mu\text{m}$ and the estimation of the needed parameter combination (N, E) for their fabrication is shown in Fig. 6.

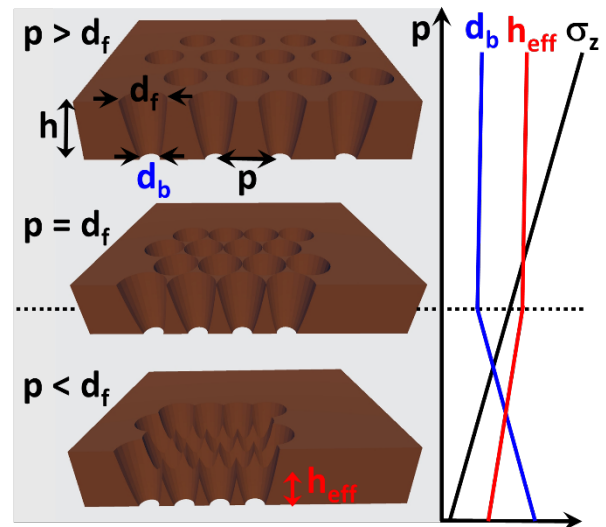


Fig. 7 Schematic illustration of the resultant structure dependent on the pore distance p . The reduction of the pore distance ($p < d_f$) result in an increasing of the rear side hole diameter d_b and in the reduction of the effective foil thickness h_{eff} . Further, the decreasing of the hole distance result in the reduction of the mechanical stability like a decreasing of the ultimate tensile strength σ_z .

The estimation predicted that the maximum areal pore density increased at increasing number of laser pulses. That means based on Eq. 6-8, a large areal pore density can be achieved at low laser pulse energy and high number of laser pulses. However, the experimental results predicted that pore distances below the front side hole diameter is possible. The reduction of the pore distance below the front side hole diameter result in an increasing of the rear side hole diameter (see Fig. 5 and Fig. 6) which can be explained by the reduction of the effective foil height ($h_{eff} < h$) due to the overlap on the front side. Further, the reduction of the hole distance result in the reduction of mechanical stability of the laser-treated foils. This process limits the achievable areal pore density. The next step, the quantitative analysis of the mechanical stability dependent on the hole distance and the areal pore density by means of tensile tests is necessary, respectively.

• Hole shape

The shape of the laser-induced pore is defined by the laser beam profile; hence the applied Gaussian laser beam results in a circular hole at the front side of the PI foil (see Fig. 1 and 2). An almost circular shaped hole can be found also at low laser energies at the rear side (see Fig. 4 (bottom)). However, the rear side holes show a deviation from the circular shape at higher laser energies (see Fig. 5). In relation to Fig. 1, showing a conic pore in the PI foil, the roughness of the side walls increases towards the exit hole. This suggests an intensity modulation of the laser beam inside the hole that can be originate from reflection and scattering at the side walls. This pore sidewall roughness results shortly before opening the hole in a varying residual foil thickness. Both, the thickness variation and the intensity modulation results in the formation of an arbitrary, jagged rear side holes. The jagged edge further can be discussed with the rupture of the residues foil at the thinnest sections. Any inhomogeneity of the material results in local differences of the ablation rate and in consequence in thickness variations of the residual layer. The improving of the rear side hole shape can be achieved by a proportional material removal process

4. Conclusion and Outlook

The ps-laser ablation of a polyimide foil with a gaussian laser beam was studied for drilling of pores and pores arrays forming perforated membranes. From the experimental determined correlations between process parameters laser fluence, pulse number, and foil thickness etc. and the pores array characteristics like rear/front side diameter, hole conicity and areal hole density a simple empirical model was extracted based on laser ablation mechanism. For 13 μm thick polyimide foils and 11 μm laser spot size

- a minimal rear side pores diameters of below 1 μm ,
- a typical derivation of the hole diameter of $\leq 10\%$ (for pore size $\geq 1\ \mu\text{m}$), and
- a areal holes density of $\sim 12\%$ has been achieved.

With optimal processing parameters membranes with 2.5 μm pores of a deviation of 0.2 μm and an open pore area of 12 % can be realized. The holes density is limited by the circular pores shape and the holes conicity. Lower laser fluences cause a higher conicity and lower holes density. The produced membranes have a high potential for use as micro-biological filters due to the precise pore size that can be adjusted in the micrometer range and the high areal pore density.

Acknowledgements

We appreciate the support by the BMWi (Bundesministeriums für Wirtschaft und Energie) as part of ZIM (Zentrales Innovationsprogramm Mittelstand) at Grant No. ZF4135604BA8.

References

[1] A. Shiohara, B. Prieto-Simon, and N.H. Voelcker: *J. Mat. Chem. B*, 9, (2021) 2129.
 [2] A.A. Serafetinides, M.I. Makropoulou, C.D. Skordoulis, and A.K. Kar: *Appl. Surf. Sci.*, 180, (2001) 42.
 [3] S. Ravi-Kumar, B. Lies, X. Zhang, H. Lyu, and H. Qin: *Polym Int*, 68, (2019) 1391.
 [4] P. Lorenz, L. Bayer, M. Ehrhardt, K. Zimmer, and L. Engisch: *Proc. SPIE*, Vol. 9351, (2019) 935119.

[5] D. Bäuerle, "Laser Processing and Chemistry", (Springer, Berlin, Heidelberg, New York, 2011) .
 [6] P.E. Dyer: *Applied Physics A*, 77, (2003) 167.
 [7] P.E. Dyer, M. Pervolaraki, and T. Lippert: *Appl. Phys. A*, 80, (2005) 529.
 [8] J. Hrabovsky, C. Liberatore, I. Mirza, J. Sladek, J. Beranek, A.V. Bulgakov, and N.M. Bulgakova: *Interfacial Phenom. Heat Transf.*, 7, (2019) 113.
 [9] T. Lippert, M. Hauer, C.R. Phipps, and A. Wokaun: *Appl. Phys. A*, 77, (2003) 259.
 [10] A. Lasagni, M. Cornejo, F. Lasagni, and F. Muecklich: *Adv. Eng. Mater.*, 10, (2008) 488.
 [11] I. Antanavičiūtė, L. Šimatonis, O. Ulčinas, A. Gadeikytė, B. Abakevičienė, S. Tamulevičius, V. Mikalayeva, V.A. Skeberdis, E. Stankevičius, and T. Tamulevičius: *J. Tissue Eng. Regen. Med.* 12 (2018) e760.
 [12] M. Ohnishi, H. Shikata, M. Sakakura, Y. Shimotsuma, K. Miura, and K. Hirao: *Appl. Phys. A*, 98, (2009) 123.
 [13] D. Bäuerle, M. Himmelbauer, and E. Arenholz: *J. Photochem. Photobiol.*, 106, (1997) 27.
 [14] K.C. Yung and D.W. Zeng: *Surf. Coat. Technol.*, 145, (2001) 186.
 [15] A. Braun, K. Zimmer, and F. Bigl, *Appl. Surf. Sci.*, 154-155, (2000) 73.
 [16] G. Danev, E. Spassova, J. Assa, J. Ihlemann, and D. Schumacher: *Appl. Surf. Sci.* 168 (2000) 162.
 [17] C.T. Pan, H. Yang, and M.K. Wei: *Int. J. Adv. Manuf.*, 34, (2007) 889.
 [18] K. Zimmer, R. Bohme, T. Stephan, C. Scheit, and A. Braun: *Appl. Surf. Sci.*, 255, (2009) 9869.
 [19] W. Zhao and L. Wang: *Polymers*, 10, (2018) 1390.
 [20] Y. Liu, T. Li, M. Xu, W. Zhang, Y. Xiong, L. Nie, Q. Wang, H. Li, and W. Wang: *Lab Chip*, 19, (2018) 68.
 [21] I. Antanavičiūtė, L. Šimatonis, O. Ulčinas, A. Gadeikytė, B. Abakevičienė, S. Tamulevičius, V. Mikalayeva, V.A. Skeberdis, E. Stankevičius, and T. Tamulevičius: *J. Tissue Eng. Regen. Med.*, 12, (2018) e760.
 [22] J.M. Liu: *Opt. Lett.*, 7 (1982) 196.
 [23] M.C. Gower, E. Davies, and A.S. Holmes: *J. Laser Micro Nanoeng.*, 8 (2013) 56.
 [24] W.K.C. Yung, J.S. Liu, H.C. Man, and T.M. Yue: *J. Mater. Process. Technol.*, 101, (2000) 306.
 [25] Y. Jee, M.F. Becker, and R.M. Walser: *J. Opt. Soc. Am. B*, 5, (1988) 648.
 [26] F. Di Niso, C. Gaudioso, T. Sibillano, F.P. Mezzapesa, A. Ancona, and P.M. Lugarà: *Phys. Procedia*, 41, (2013) 698.
 [27] S. Baudach, J. Bonse, and W. Kautek, *Appl. Phys. A*, 69 (1999) S395.
 [28] P. Heszler, Z. Bor, and G. Hajos: *Appl. Phys. A*, 49 (1989) 739.
 [29] J. Krüger and W. Kautek: "Polymers and Light" ed. by T.K. Lippert, (Springer, Berlin, Heidelberg, 2004) p. 247.

(Received: November 3, 2021, Accepted: January 21, 2022)